Available online at www.sciencedirect.com
SCIENCE DIRECT®
International Journal of Machine Tools & Manufacture 44 (2004) 1151–1161
INTERNATIONAL JOURNAL OF MACHINE TOOLS & MANUFACTURE DESIGN, RESEARCH AND APPLICATION
www.elsevier.com/locate/ijmactool

Structural modeling of end mills for form error and stability analysis

E.B. Kivanc, E. Budak *

Faculty of Engineering and Natural Sciences, Sabanci University Orhanli Tuzla, 34956 Istanbul, Turkey

Received 20 February 2004; received in revised form 25 March 2004; accepted 8 April 2004

Abstract

Structural modeling of end mills is crucial for predicting deflections and vibrations in milling processes. End mill geometry is very complex which makes the use of simple beam models inaccurate. Stiffness and frequency response function (FRF) measurements need to be performed to identify the static and dynamic properties experimentally. This can be very time consuming considering the number of tool–tool holder combinations in a production facility. In this paper, methods for modeling structural properties of milling tools are presented. Static and dynamic analysis of tools with different geometry and material are carried out by finite element analysis (FEA). Some practical equations are developed to predict the static and dynamic properties of tools. Receptance coupling and substructuring analyses are used to combine the dynamics of individual component dynamics. In this analysis, experimental or analytic FRFs for the individual components are used to predict the final assembly's dynamic response. Clamping parameters between the tool and the tool holder may effect the results significantly. These parameters are also identified from the measurements. The effects of changes in tool parameters and clamping conditions are evaluated. The predictions are verified by the measurements for different conditions.

Keywords: Milling; Deflections; Stability

1. Introduction

Tolerance integrity and surface quality of machine parts are of prime importance in milling processes as well as productivity. Static and dynamic deformations of machine tool, tool holder and cutting tool play an important role in tolerance integrity and stability in a machining process affecting part quality and productivity. Excessive static deflection may cause tolerance violations whereas chatter vibrations result in poor surface finish. Cutting force, surface finish and cutting stability models can be used to predict and overcome these problems. This would require static and dynamic characteristics of the structures involved in a machining system [1]. Considering great variety of machine tool configurations, tool holder and cutting tool geometries, analysis of every case can be quite time consuming and unpractical. These properties are usually obtained experimentally using stiffness measurements and modal analysis [1–3]. In this study, generalized equations are presented which can be used for predicting the static and dynamic properties of milling system components. Due to its wide use in industry, milling process is considered, however, similar approaches can be applied to other machining operations as well. The structural models presented in this paper, together with the process models, can be used in the development of a virtual machining system where the physics of the process can be simulated in addition to the geometry and tool path in conventional CAD/CAM applications.

Modeling of milling process has been the subject of many studies some of which are summarized by Smith and Tlusty [4]. The focus of these studies has mostly been on the modeling of cutting geometry and force, stability and prediction of part quality [5–9]. The mechanistic approach has been widely used for the force predictions and also has been extended to predict deflections and form errors [6–7]. An alternative method is to use mechanics of cutting approach in

* Corresponding author. Tel.: +90-216-483-9519; fax: +90-216-483-9550.
E-mail address: ebudak@sabanciuniv.edu (E. Budak).

0890-6955/$ - see front matter © 2004 Elsevier Ltd. All rights reserved.
doi:10.1016/j.ijmachtools.2004.04.002

Nomenclature

A	area (mm^2)
D	diameter (mm)
E	modulus of elasticity (MPa)
F	applied force (N)
I	second moment of inertia (mm^4)
L	length (mm)
G_{mn}	assembly receptance FRF element
H_{mn}	individual receptance FRF element
C	viscous damping coefficient (N s/m)
k	stiffness (N/m)
ω	frequency (Hz)
ρ	density (kg/m^3)
fd	flute depth
R, S	mode shapes
k_x, k_θ	linear and rotational connection stiffness
c_x, c_q	linear and rotational connection damping

Subscripts

m	coordinate
n	location of the force

determining milling force coefficients as used by Armarego and Whitfield [10].

Another major limitation on productivity and surface quality in milling is chatter vibrations which develop due to dynamic interactions between the cutting tool and workpiece. Chatter vibrations result in poor surface finish and reduced tool life. Koenigsberger and Tlusty [3] and Tobias [11] identified the most powerful source of self-excitation which is associated with the structural dynamics of the machine tool and the feedback between the subsequent cuts on the same cutting surface resulting in regeneration of waviness on the cutting surfaces. In the early milling stability analysis, Tlusty used an approximate analytical model [3] and time domain simulations [12] for predicting of chatter stability in milling. Minis et al. [13] used Floquet's theorem and the Fourier series for the formulation of the milling stability, and numerically solved it using the Nyquist criterion. Budak and Altintas [14] developed a stability method which leads to analytical determination of stability limits. The stability of low radial immersion milling has been investigated and modeled in [15,16] where cases for the doubled number of stability lobes are presented. These methods can be used to generate stability diagrams from which stable cutting conditions, and spindle speeds resulting in much higher stability can be determined for given work material, tool geometry and transfer functions.

Demonstrations of cutting model implementation in CAD/CAM systems have been done in several. Altintas and Spence [17] and Yazar et al. [18] demonstrated that force models could be used to predict form errors and optimize feedrates based on simulation at the CAD/CAM stage. Weck et al. [19] demonstrated determination of chatter free milling conditions in a commercial CAD/CAM software. Cutting force coefficients and tool dynamics were needed for these simulations, which were determined experimentally. Generation of an orthogonal cutting database for a work material as Budak et al. [20] did reduces the amount of experiments, and thus makes implementation of force models in CAD/CAM more practical.

There is a need for more practical determination of structural properties of the cutting tool for a virtual machining system. Kops and Vo [21] determined an equivalent diameter for end mill based on finite element analysis (FEA) in order to be able to use beam equations for deflection calculations, which eliminates stiffness measurements for each tool. Schmitz [22,23] used substructuring methods to predict the dynamics of tool holder–end mill assembly using beam component modes.

In this paper, a precise modeling of tool structure is presented for accurate determination of form errors and stability limits. End mill geometry is very complicated, thus in general, beam approximations do not provide accurate stiffness and transfer function predictions. Both FEA and analytical methods have been used for static and dynamic analysis of end mills. Dynamics of end milling systems are modeled using two different approaches by a cantilevered beam approximation and by including tool holder dynamics as well as clamping flexibility. Simplified, but accurate equations are presented for end mills, which can be used in CAD/CAM systems for form error and stability limit calculations. The analytical results are verified numerically and experimentally.

2. Deflection analysis of end mills

The main objective of the static analysis is to determine the deflection of end mills under milling forces. For static deflection analysis of end mills, the tool holder is assumed to be rigid and the cantilever beam model is used. However, the holder and clamping stiffness can also be included in the analysis if they are known [2]. End mill deflections can be approximated using the beam model. The loading and boundary conditions of the end mill used in the model are shown in Fig. 1, where $D1$ is the mill diameter, $D2$ is the shank diameter, $L1$ is the flute length, $L2$ is the overall length, F is the point load, $I1$ is the moment of inertia of the part with flute and $I2$ is the moment of inertia of the part without flute.

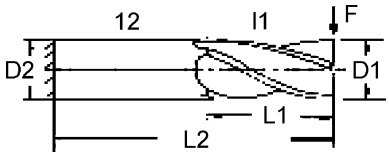

Fig. 1. Loading and boundary conditions of the end mill.

The moment–area theorems are used to determine the maximum deflection at the end of the cutting tool [24].

$$y_{\max} = \frac{FL1^3}{3EI1} + \frac{1}{6}\frac{FL1(L2-L1)(L2+2L1)}{EI2} + \frac{1}{6}\frac{FL2(L2-L1)(2L2+L1)}{EI2} \quad (1)$$

The deflections can be approximated using an equivalent diameter in Eq. (1) as suggested in [21]. However, the accuracy of the predictions can be improved by including the flute geometry in the formulation as formulated in the next section.

2.1. Moment of inertia

Models of 4-flute, 3-flute and 2-flute end mills are used to determine the moment of inertias analytically. Due the complexity of the cutter cross section along its axis, the inertia calculation is the most difficult aspect of the static analysis. The cross sections of the end mills are as shown in Fig. 2.

In order to determine the inertia of the whole cross section, inertia of region 1 is first derived, and inertia of the other regions are obtained by transformation. The total inertia of the cross section is then obtained by summing the inertia of all regions. The effect of the arcs due to flute depths (fd) is added to total inertia. Regions for 4-flute, 3-flute and 2-flute are shown in Fig. 3.

The inertia of region 1 is derived by computing equivalent radius R_{eq} in terms of the radius r of the arc, position of the center of the arc (a) and θ. Using cosine law, the equivalent radius R_{eq} for region 1 of 4-flute, 3-flute and 2-flute end mill with respect to

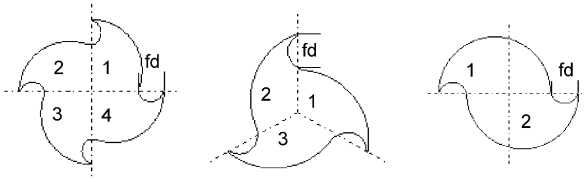

Fig. 2. Cross sections of the 4-flute, 3-flute and 2-flute end mills.

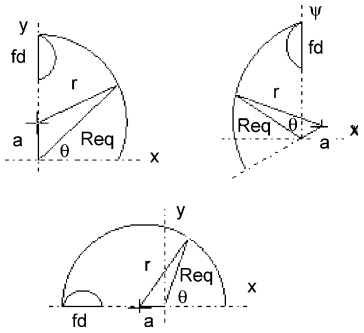

Fig. 3. Region 1 of 4-flute, 3-flute and 2-flute end mill.

x- and y-axes as [25]

$$\begin{aligned}
R_{\text{eq4-flute}}(\theta) &= a\cdot\sin(\theta) + \sqrt{(r^2-a^2)+a^2\cdot\sin^2(\theta)} \qquad 0<\theta\le\pi/2\\
R_{\text{eq3-flute}}(\theta) &= a\cdot\cos\left(\theta+\frac{\pi}{3}\right) + \sqrt{(r^2-a^2)+a^2\cdot\cos^2\left(\theta+\frac{\pi}{3}\right)} \quad 0<\theta\le 2\pi/2\\
R_{\text{eq2-flute}}(\theta) &= -a\cdot\cos(\theta) + \sqrt{(r^2-a^2)+a^2\cdot\cos^2(\theta)} \qquad 0<\theta\le\pi
\end{aligned} \quad (2)$$

The moment of inertia of region 1 of a 4-flute end mill about x- and y-axes can be written as

$$\begin{aligned}
I_{xx4-\text{flute}} &= \left[\int_0^{\pi/2}\int_0^{R_{\text{eq4-flute}}(\theta)} \rho^3\cdot\sin^2(\theta)\,\mathrm{d}\rho\,\mathrm{d}\theta\right] - \left[\frac{1}{8}\pi\left(\frac{\text{fd}}{2}\right)^4 + \frac{\pi(\text{fd}/2)^2}{2}\left(r+a-\frac{\text{fd}}{2}\right)^2\right]\\
I_{yy4-\text{flute}} &= \left[\int_0^{\pi/2}\int_0^{R_{\text{eq4-flute}}(\theta)} \rho^3\cdot\cos^2(\theta)\,\mathrm{d}\rho\,\mathrm{d}\theta\right] - \left[\frac{1}{8}\pi\left(\frac{\text{fd}}{2}\right)^4\right]
\end{aligned} \quad (3)$$

where $0<\rho\le \mathrm{R}_{eq}(\theta)$. The same formulation can be written for region 1 of the 3-flute and 2-flute tool. After transforming the inertia of region 1, the total inertias are found as follows

$$\begin{aligned}
I_{xx4-\text{flute,TOT}} &= I_{yy4-\text{flute,TOT}} = 2(I_{xx4-\text{flute}} + I_{yy4-\text{flute}})\\
I_{xx3-\text{flute,TOT}} &= I_{yy3-\text{flute,TOT}} = 1.5(I_{xx4-\text{flute}} + I_{yy4-\text{flute}})\\
I_{xx2-\text{flute,TOT}} &= 2(I_{xx2-\text{flute}}),\quad I_{yy2-\text{flute,TOT}} = 2(I_{yy2-\text{flute}})
\end{aligned} \quad (4)$$

2.2. FE modeling and analysis of cantilever tool

In order to verify and improve the accuracy of analytical model predictions, FEA is also used for tool deflections. For parametric and geometric solid modeling, FE modeling and analysis, I-DEAS® is used. Many simulations were performed for end mills with

different material, flute diameter, shank diameter, flute length, overall length and number of teeth. Modulus of elasticity and density are 200 and 605 GPa, and 8600 and 12,500 kg/m^3 for HSS and carbide tools, respectively. The Poisson's ratio is 0.3 for both the tool materials.

FE method is used to determine deformations of the tool when a point force is applied at its free end. The comparison of some deflections by analytical solutions and FEA are shown in Table 1. Approximately 60 tools were tested.

Modeling and FEA can be unpractical and time consuming for each tool configuration in a virtual machining environment. Therefore, simplified equations are generated to predict deflections of tools for given geometric parameters and density. The static characteristics of end mills can easily be

$$\text{deflection}_{\max} = C\frac{F}{E}\left[\frac{L1^3}{D1^4} + \frac{(L2^3 - L1^3)}{D2^4}\right]^N \tag{5}$$

where F is the applied force and E is the modulus of elasticity (MPa) of the tool material. The geometric properties of the end mill are in mm. The constant C is 9.05, 8.30 and 7.93 and N is 0.950, 0.965 and 0.974 for 4-flute, 3-flute and 2-flute cutters, respectively.

A 4-flute high speed steel long slender end mill is selected to demonstrate the accuracy of analytical results. The mill and shank diameter is 6 mm, the flute length is 38 mm and the gauge length is 75 mm. A force is applied to end point of the tool and measured by dynamometer and displacements at the two points of the tool are measured by dial gage. Total displacement of the tool is equal to summation of clamping displacement, beam displacement and rotational displacement. Rotational displacement is assumed to be zero. The experimental beam stiffness is 75 N/mm and the stiffness of the tool, which is calculated by using analytical equation, is 70.5 N/mm. The agreement between two stiffness values is satisfactory.

3. Dynamic analysis of the tool

Dynamics of the tool is required for the stability analysis and stability limit prediction. Two different cases will be considered for analytical modeling of the end mill dynamics. For slender end mills where the dynamics is mostly dominated by the tool modes, flexible tool–rigid holder model will be used. A general case will also be presented where the tool, tool holder, spindle and the clamping stiffness and damping are also included.

3.1. Flexible tool–rigid holder

3.1.1. Analytical model

Dynamic analysis is used to determine mode shapes and natural frequencies of the cutting tool structures. A modeling method for transverse vibrations of an end mill is developed. End mill is a segmented beam, one segment for the part with flute and the other segment for the shank. The beam model with two different geometric segments is shown in Fig. 4 where $I1$, $I2$ and $A1$, $A2$ are the moment of inertias and the areas of the segments, respectively. $R(x)$ and $S(y)$ are the mode shapes, and $w1(x, t)$ and $w2(x, t)$ are the displacement functions. The governing equations of motion, neglecting the rotational inertia and shear formation, can be converted into the well-known Euler–Bernoulli equations:

$$\begin{aligned} EI1\frac{\mathrm{d}^4R}{\mathrm{d}x^4} - \rho A1\omega^2 R = 0, \quad 0 \le x \le L1 \\ EI2\frac{\mathrm{d}^4S}{\mathrm{d}y^4} - \rho A2\omega^2 S = 0, \quad 0 \le y \le L2 \end{aligned} \tag{6}$$

Table 1
Results of the analytic equations and FE solutions

Flutes	Material	$D1$ (mm)	$D2$ (mm)	$L1$ (mm)	$L2$ (mm)	y-Analytical (mm), force = 50 N	y-FEA (mm), force = 50 N	Difference (%)
4	HSS	6	6	13	57	0.248844	0.251768	1.16
3	HSS	6	6	13	57	0.245466	0.250252	1.91
2	HSS	6	6	13	57	0.244309	0.249888	1.23
4	HSS	10	13	22	72	0.027316	0.028412	3.86
3	HSS	10	13	22	72	0.025169	0.026517	5.08
2	HSS	10	13	22	72	0.024448	0.026007	5.99
4	Carbide	16	16	32	92	0.007281	0.007580	3.94
3	Carbide	16	16	32	92	0.006950	0.007315	4.99
2	Carbide	16	16	32	92	0.006777	0.007163	5.38
4	Carbide	20	20	38	104	0.004368	0.004630	5.66
3	Carbide	20	20	38	104	0.004138	0.004463	7.27
2	Carbide	20	20	38	104	0.004062	0.004409	7.86

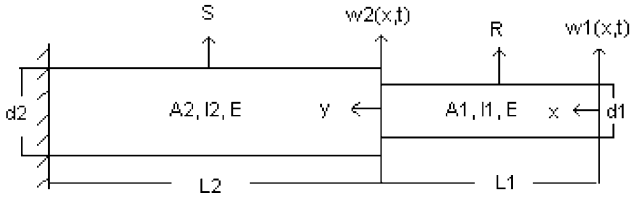

Fig. 4. The geometry of the beam with two different geometric segments.

where E is the modulus of elasticity and ρ is the density. The solution of Eq. (6) can be expressed as

$$R(x) = A1 \cdot \cosh(\beta x) + A2 \cdot \sinh(\beta x) + A3 \cdot \cos(\beta x) + A4 \cdot \sin(\beta x)$$
$$S(x) = A5 \cdot \cosh(\alpha x) + A6 \cdot \sinh(\alpha x) + A7 \cdot \cos(\alpha x) + A8 \cdot \sin(\alpha x) \quad (7)$$

where $A1$, $A2$, $A3$, $A4$, $A5$, $A6$, $A7$ and $A8$ are arbitrary constants. It is necessary to accompany the general solutions with the boundary conditions. The boundary conditions are as follows. At $x = 0$ (i.e. at the free end), bending moment and shear force are defined as

$$\frac{d^2R(0)}{dx^2} = 0, \quad \frac{d^3R(0)}{dx^3} = 0 \quad (8)$$

At $x = L1$ and $y = 0$ the continuity equations for displacement, slope, moment and shear force are as follows:

$$R(L1) = S(0), \quad \frac{dR(L1)}{dx} = \frac{dS(0)}{dy},$$
$$\frac{d^2R(L1)}{dx^2} = \frac{d^2S(0)}{dy^2}, \quad \frac{d^3R(L1)}{dx^3} = \frac{d^3S(0)}{dy^3} \quad (9)$$

At $y = L2$ (i.e. at the fixed end) displacement and slope equations:

$$S(L2) = 0, \quad \frac{dS(L2)}{dy} = 0 \quad (10)$$

These eight conditions defined by Eqs. (8)–(10) are sufficient to solve for the eight arbitrary constants. The equations involving these constants can be written in the following form:

$$[C]\{A\} = 0$$

where A_j is the vector of the eight arbitrary constants and the coefficient matrix $[C]$ is of dimension (8×8), and is given by

The characteristic equation is determined if $|C| = 0$. The natural frequencies are computed from the solution of characteristic equation as

$$\omega = (\beta L1)\sqrt{\frac{EI1}{\rho A1 L1^4}} \quad \text{or} \quad \omega = (\alpha L2)\sqrt{\frac{EI2}{\rho A2 L2^4}} \quad (11)$$

The mode shapes according to the frequencies are obtained by combining $R(x)$ and $S(y)$ from Eq. (7).

3.1.2. FE solution

In I-DEAS®, models are built to define geometry, material properties, element types and constraints for end mills. Natural frequencies and mode shapes are obtained using FEA. Many end mills with different material and geometric parameters are analyzed. In case of a 2-flute end mill, lateral and vertical bending

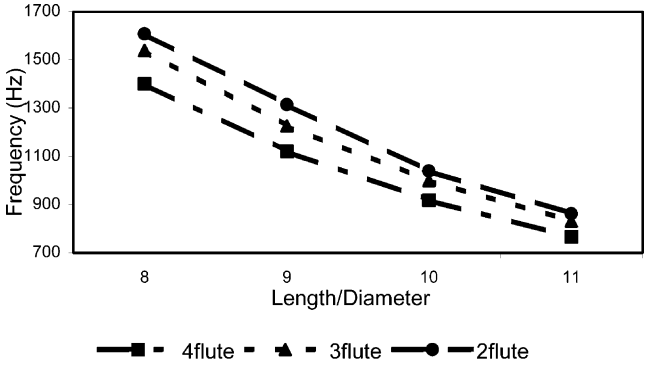

Fig. 5. Relationship between natural frequencies (mode1) of HSS tool and tool length/diameter ratio.

$$[C] = \begin{bmatrix} 1 & 0 & -1 & 0 & 0 & 0 & 0 & 0 \\ 0 & 1 & 0 & -1 & 0 & 0 & 0 & 0 \\ \cosh(\beta L1) & \sinh(\beta L1) & \cos(\beta L1) & \sin(\beta L1) & -1 & 0 & -1 & 0 \\ \sinh(\beta L1) & \cosh(\beta L1) & -\sin(\beta L1) & \cos(\beta L1) & 0 & \frac{-\alpha}{\beta} & 0 & \frac{-\alpha}{\beta} \\ \cosh(\beta L1) & \sinh(\beta L1) & -\cos(\beta L1) & -\sin(\beta L1) & \frac{-\alpha^2}{\beta^2} & 0 & \frac{\alpha^2}{\beta^2} & 0 \\ \sinh(\beta L1) & \cosh(\beta L1) & \sin(\beta L1) & -\cos(\beta L1) & 0 & \frac{-\alpha^3}{\beta^3} & 0 & \frac{\alpha^3}{\beta^3} \\ 0 & 0 & 0 & 0 & \cosh(\alpha L2) & \sinh(\alpha L2) & \cos(\alpha L2) & \sin(\alpha L2) \\ 0 & 0 & 0 & 0 & \sinh(\alpha L2) & \cosh(\alpha L2) & -\sin(\alpha L2) & \cos(\alpha L2) \end{bmatrix}$$

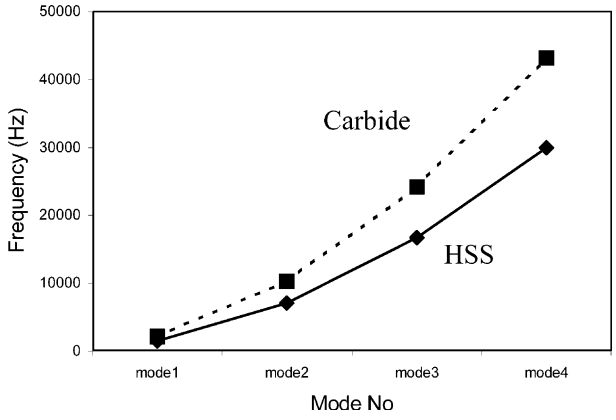

Fig. 6. Comparison between carbide and HSS natural frequencies.

frequencies are different as the cutter cross section is not symmetric with respect to x and y axes.

As the tool length/diameter ratio increases, the natural frequency of the tool decreases (Fig. 5). 2-flute cutters have the greatest natural frequency and 4-flute cutters have the least because of the cross section. The carbide tools have higher natural frequency than HSS tools because of their high modulus of elasticity (Fig. 6).

3.2. Tool dynamics including machine flexibility

3.2.1. Receptance coupling substructure analysis for tool dynamics

In this model, the complete machine structure is divided into two parts: tool and tool holder/spindle. The description of the assembly model and the connection parameters are shown in Fig. 7 [20]. The four connection parameters (linear and torsional springs and dampers) must be determined to predict tool point frequency response function (FRF). According to these parameters, tool and tool holder/spindle FRFs are coupled using receptance coupling substructure analysis (RCSA). RCSA is a very efficient method to predict dynamic response of tools without measurements for each tool, tool holder and spindle combination. In this study, the analytical model developed for the tool dynamics given in Section 3.1 is used together with RCSA to determine the total dynamics of the machine.

In RCSA, each component of the assembly must be tested separately to determine the component FRFs.

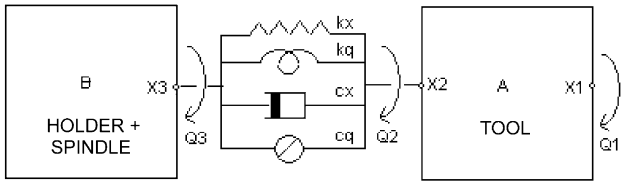

Fig. 7. Tool and tool holder/spindle assembly.

Nevertheless, this is only possible if the impact tests on the individual parts provide enough information to predict accurately the dynamic properties of the assembled structure. In case of low natural frequency modes, the dynamics at the tool and tool holder/spindle interface might not be adequately represented in the modal data. Furthermore, in many cases the measurement of component dynamics is not practical which is the case for free–free end mill.

The direct and cross free–free FRFs of the tool are calculated analytically using the model presented in this paper. In the formulation, the component modes are represented by H whereas G is for the assembly FRFs. Direct and cross deflection receptance terms (H_{11}, H_{22} and $H_{12} = -H_{21}$), displacement under applied force (L_{mn}), rotation under applied force (N_{mn}) and the rotation under applied moment (P_{mn}) for the component A are derived analytically [22]. For the calculations, density (ρ), elastic modulus (E), viscous damping coefficient (c) and second moment of inertia (I) are required. In the static analysis section, an analytic equation for the maximum displacement at the tool tip was derived (Eq. (1)) which can be used to determine the stiffness of the tool. The effective diameter of the tool and the second moment of inertia can be calculated using the analytical equations developed in Section 1 for segmented beam with different moments of inertias and the cantilever beam equation of the uniform cylinder. The mass of the tool can then be determined using the natural frequency and stiffness both from analytic equations. The damping ratios for many HSS and carbide tools have been determined experimentally. Average values of $\zeta = 0.018$ and $\zeta = 0.012$ have been obtained from experimental data for HSS and carbide tools, respectively. By using these dynamic properties, approximate c values are estimated. Note that c values determined this way includes the damping of the tool only as they are identified from end mill's component mode dynamics. These damping ratio values can then be used in the analysis of different tools.

For the tool holder/spindle component, the direct deflection receptance term (H_{33}) is measured at the intersection location by impact test. L_{33}, N_{33} and P_{33} are assumed to be zero. The holder and spindle dynamic properties can also be determined using FEA [26,27]. However, the number of spindle/holder combinations for milling tools is much more limited on a machining center, and thus they can be measured and used for different end mill combinations.

Finally, after RCSA for the complete structure, the analytical displacement/force relationship at the tool tip (G_{11}), which is required for stability and chatter

avoidance, is given as [20]:

$$G_{11} = \frac{X_1}{F_1} = H_{11} - H_{12}E_1^{-1}E_2 - L_{12}E_3^{-1}((k_qN_{21} + c_qN'_{21}) - E_4E_1^{-1}E_2) \quad (12)$$

where

$$E_1 = (k_xH_{33} + k_xH_{22} + c_xH'_{33} + c_xH'_{22} + 1) - E_3^{-1}E_4(k_xL_{33} + k_xL_{22} + c_xL'_{33} + c_xL'_{22})$$

$$E_2 = (k_xH_{21} + c_xH'_{21}) - E_3^{-1}(k_qN_{21} + c_qN'_{21}) \times (k_xL_{33} + k_xL_{22} + c_xL'_{33} + c_xL'_{22})$$

$$E_3 = k_qP_{33} + k_qP_{22} + c_qP'_{33} + c_qP'_{22} + 1$$

$$E_4 = k_qN_{33} + k_qN_{22} + c_qN'_{33} + c_qN'_{22}$$

3.2.2. Identification of connection parameters

In experiments, the tool point FRFs (G_{11}) of the tool/tool holder/spindle assembly are measured for different tools. From RCSA point of view, this resultant FRF includes the dynamics of tool holder at the tip, clamping and the tool. From the analytical component modes presented here, and the experimental data, all these except the clamping parameters are known. Therefore, the clamping stiffness and damping can be identified from tool point FRF. This should be done using least squares error minimization method in order to minimize the overall error in the considered frequency range for the FRF. The connection parameters (k_x, k_q, c_x, c_q) are determined using *lsqnonlin* command of Matlab Optimization Toolbox [28,29]. *Isqnonlin* solves nonlinear least squares problems, including nonlinear data fitting. $X =$ *lsqnonlin (fnctn,* X_o*)* starts at a point X_0 and finds a minimum to the sum of squares of the functions described in *fnctn*. Our syntax is [X, *resnorm*, *residual*, *exitflag*, *output*] = *lsqnonlin* (*fnctn*, X_0, lb, ub, options). The solution is always in the range $lb \leq X \leq ub$. The optimization parameters (*max iteration number, max function evaluation number, tolerances for function and X values*) are specified in the structure options. The value of the residual for a solution X, the value *exitflag* (0,1) that describes the exit condition and the structure output that contains information about the optimization are returned. According to the calculated spring and damper parameters, the tool point FRF of the assembly is predicted analytically using Eq. (12). The measurements and predictions for G_{11} are compared in the next section.

The knowledge of the FRF of the tool point can be used to predict the stability lobe diagrams. The critical axial depth of cut can be determined easily from the stability lobes. Therefore, for a given end mill on a particular machining center, the stable milling conditions can be determined completely analytically. This is very useful information in a virtual machining environment, which is the next step in CAM.

4. Experimental verification

4.1. Tool deflection and maximum surface error

Milling forces can be modeled for given cutting and cutter geometry, cutting conditions, and work material [1]. The cutting forces in both directions can be used to determine milling tool deflections. In milling, the surface is generated when the cutting flutes intersect the finished surface. Thus, deflections of the tool at those points are imprinted as surface form errors. The simulation of the surface form error in milling is given in [2].

The stiffness of an end mill can be calculated using the analytic model. The stiffness values are used to predict the maximum surface error generated by the end mill. For surface error calculation, the cutting forces are determined according to work material properties, cutting and tool conditions in [2] using the milling force model [1]. The results are verified using the experimental results in [2]. 4-flute high speed steel end mill with 30° helix angle is used for the comparison. The tool diameter is 19.05 mm and the tool gauge length is 54.5 mm. The stiffness of this tool is calculated as 12,761 N/mm. The model results agree with the experimental results (Table 2). The difference between the measured and the predicted maximum surface error (E_{max}) is less than 6%.

4.2. Flexible tool and rigid holder

4-flute carbide end-mill with long overhang is selected to demonstrate the accuracy of analytical results. The mill and shank diameter is 8 mm, the flute length is 41 mm and the gauge length is 80 mm. FRF measurement was performed to determine the transfer function of the end mill which is shown in Fig. 8. Table 3 shows the identified frequency, stiffness, damping and mass values for the end mill. For comparison with analytical model predictions, the results obtained using the cylinder approximation for the end mill are also shown in Table 3 and Fig. 8. The cylinder with the same diameter and length is used in calculations. Due to the long flute length of the tool, the cylinder approximation is very poor in this case as shown in Fig. 8. The approximation results could be improved

Table 2
Experimental and calculated maximum surface error results

Axial depth of cut (mm)	Feedrate (mm)	E_{max} experimental (mm)	E_{max} model (mm)	Difference (%)
19.05	0.14	0.0944	0.0912	3.38
15.00	0.10	0.0722	0.0677	6.23
15.00	0.06	0.0444	0.0438	1.35
15.00	0.02	0.0178	0.0167	6.18
18.00	0.02	0.0166	0.0158	4.82

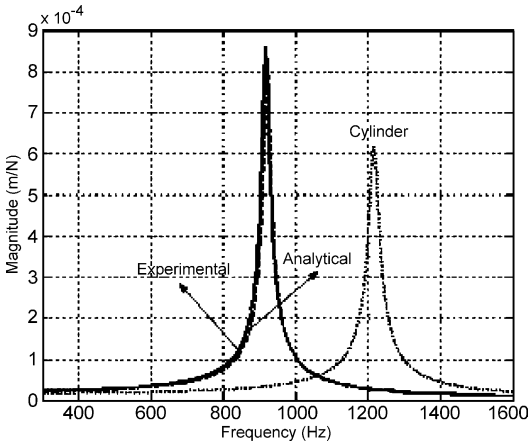

Fig. 8. Magnitude of the transfer function for the experimental, analytical and cylindrical beam methods.

Table 3
The comparison of the dynamic properties obtained from experimental, analytical and cylindrical beam methods

Transfer function	Frequency (Hz)	Stiffness (N/m)	Damping (ζ)	Mass (kg)
Experiment	935	5.11×10^5	0.012	0.0150
Analytical	922	5.50×10^5	0.012	0.0164
Cylinder	1216	7.12×10^5	0.012	0.0122

by using an effective diameter for the cylinder. As the end mills do not have circular cross sections along the flute length, the analytical solution is the most powerful approximation to find the dynamic properties. The model presented in this paper can be used to determine the dynamics of end mills for a given geometry, material and clamping conditions.

4.3. Flexible tool and flexible holder/spindle

In this section, the FRFs using analytical models and the RCSA are compared with experimental results for verification. For the identification of the interface stiffness and damping between the tool and tool holder,

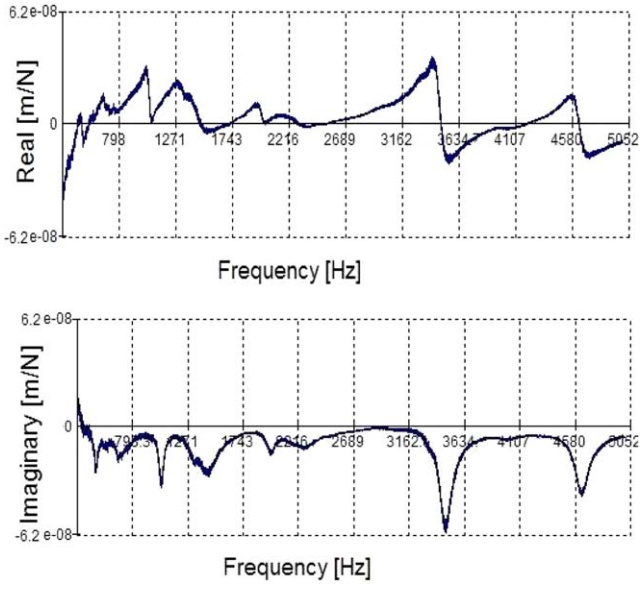

Fig. 9. Measured FRF at the tip of CAT40 tool holder/spindle combination.

different tool geometries, materials and clamping conditions are used. Contact parameters are identified and presented.

The tool holder/spindle direct FRF (H_{33}) is measured at the free end in x/y directions by using low mass accelerometer and impact hammer. The measured FRF of the CAT40 tool holder/spindle is shown in Fig. 9. The same tool holder is used with different end mills, and therefore the same FRF (H_{33}) is used in RCSA in the following examples.

4.3.1. Experiment 1—model verification

A carbide end mill with 4-flutes, 8 mm diameter, and 100 mm length is used for test. Different lengths (length to diameter ratios of 8:1, 9:1, 10:1, 11:1) are selected for the measurement. A clamping torque of 25 N m is applied on CAT40 holder. The tool effective diameter and damping coefficient were determined as 7.49 mm and 5 N s/m, respectively. After the nonlinear least square evaluation, the stiffness and damping coeffi-

Table 4
Stiffness and damping coefficients for experiment 1

	$L/D = 8$ $L_{contact} = 36$	$L/D = 9$ $L_{contact} = 28$	$L/D = 10$ $L_{contact} = 20$	$L/D = 11$ $L_{contact} = 12$
k_x (N/m)	9.036×10^6	6.885×10^6	3.614×10^6	1.304×10^6
k_q (N m/rad)	1.02×10^7	5.3×10^6	3.8×10^6	1.277×10^6
c_x (N s/m)	445	368	228	141
c_q (N m s/rad)	54.17	71.44	78.09	79.34

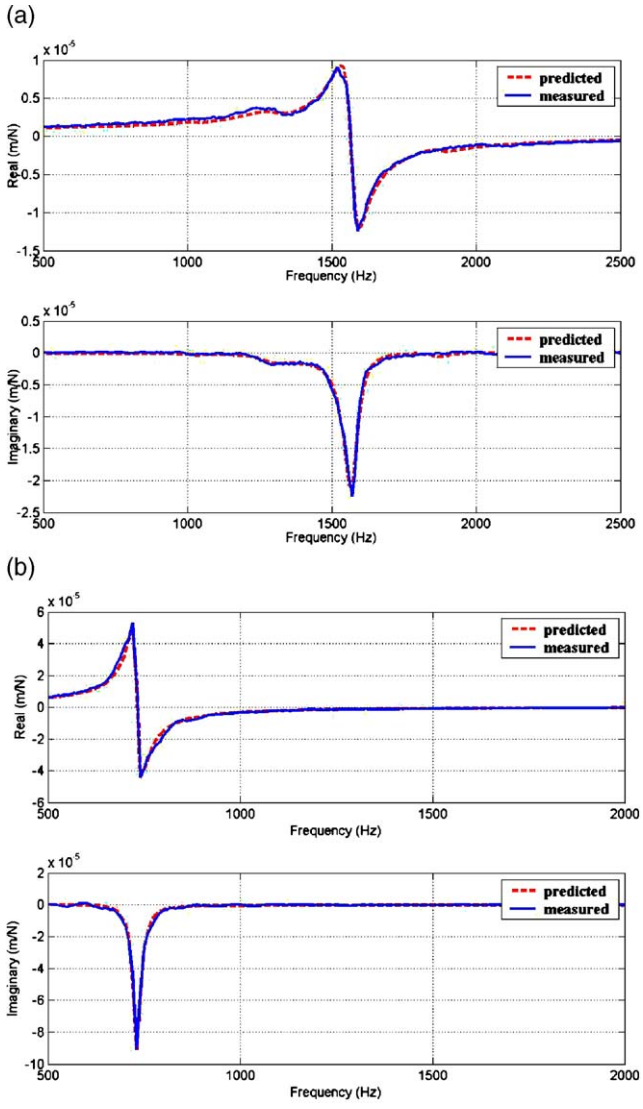

Fig. 10. Predicted and measured FRFs for experiment 1, (a) $L/D = 8$; (b) $L/D = 11$.

cients are determined as shown in Table 4. The measured and predicted FRFs using analytical component FRFs and RCSA are given for the shortest and longest tools Fig. 10. The response is governed by only the first mode of the tool, and thus only the first beam mode is used in the analytical component modes. As the contact length (L_{contact}) that is in the tool holder decreases, natural frequency decreases and flexibility increases. All connection parameters except rotational damping increase, when L_{contact} increases. The agreement between the experimental results and the predictions is satisfactory.

4.3.2. Experiment 2—holder and tool interaction

In the experiment 2, the HSS end mill, which has 16 mm diameter, 85 mm overhang and 4-flute, was mounted in CAT40 tool holder. The effective diameter of the end mill and the damping ratio were determined as 15.56 mm and 20 N s/m, respectively. The linear and rotational spring and damping coefficients for the connection between the tool and tool holder/spindle are given in Table 5. The agreement between the predicted and measured results can be seen from the Fig. 11.

Table 5
Stiffness and damping coefficients for experiment 2

k_x (N/m)	k_q (N m/rad)	c_x (N s/m)	c_q (N m s/rad)
84.8×10^5	8×10^4	1022	6.3

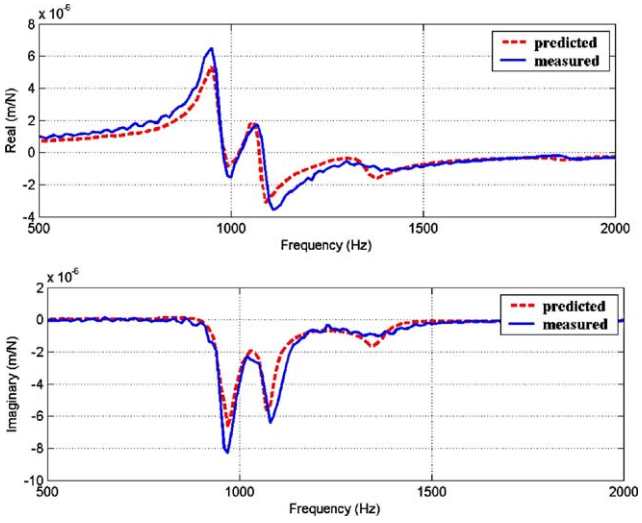

Fig. 11. Predicted and measured FRFs for experiment 2.

Because of the interaction between tool holder/spindle dynamics and the tool dynamics, two close modes are experienced as shown in the figure. The tool holder/spindle mode at the approximately 1042 Hz and the cantilever tool mode affect each other strongly resulting in two separate peaks. As a result, G_{11} is reduced which indicates that the tool holder/spindle is acting like a dynamic absorber for the tool.

4.3.3. Experiment 3—effect of clamping torque

HSS and carbide end mills with 4-flutes, 20 mm diameter, and 104 mm length are used for test. Different clamping torque values (25, 35 and 45 N m) are applied on CAT40 holder. The tool effective diameter was determined as 19.498 mm. Damping coefficients for HSS and carbide tools were 26 and 60 N s/m, respectively. The nonlinear least square evaluation is used to find the stiffness and damping coefficients for HSS and carbide tool and tool holder/spindle combination (Table 6). The stiffness and damping coefficients

Table 6
Stiffness and damping coefficients for experiment 3

	$T = 25$ N m	$T = 35$ N m	$T = 45$ N m
Carbide			
k_x (N/m)	4.56×10^7	5.27×10^7	5.72×10^7
k_q (N m/rad)	4.12×10^4	4.32×10^4	4.54×10^4
c_x (N s/m)	1642	1784	1853
c_q (N m s/rad)	0.31	0.4	0.52
HSS			
k_x (N/m)	4.46×10^7	5.00×10^7	5.58×10^6
k_q (N m/rad)	3.41×10^4	3.65×10^4	3.98×10^4
c_x (N s/m)	1401	1592	1798
c_q (N m s/rad)	0.2	0.3	0.4

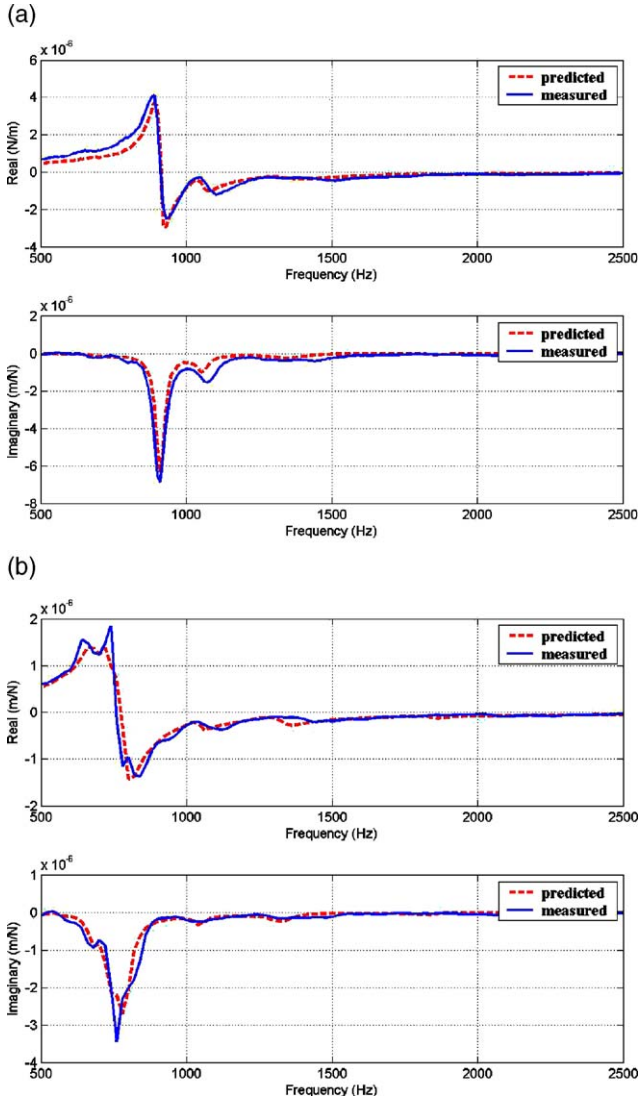

Fig. 12. Predicted and measured FRFs for experiment 3, (a) HSS; (b) carbide.

for the HSS tool and tool holder pair are slightly less than connection coefficients for carbide tool and tool holder pair. As the clamping torque applied on tool holder is increased, all coefficients increase. These values can be used to predict the effect of the clamping torque on tool dynamics and its stability.

Fig. 12 shows an example of the experimental and predicted direct tool point FRFs (G_{11}) for tool material of HSS and carbide. The overall agreement between the predicted and measured results is good.

5. Conclusion

Dynamic and static properties of milling tools are very important for machining precision and chatter stability. In general, approximate analytical or experimental results are used to determine these characteristics. Approximate results do not provide accurate information particularly for the dynamics and chatter stability. Experimental methods, on the other hand, are time consuming considering the possible number of tool and tool holder combinations, tool geometry and material in an industrial setting. The analytical models presented in this work eliminate the need for transfer function measurements for every tool assembly. The models consider the complex geometry of flutes in development of cross sectional properties. End mills have flutes and unfluted sections, which further complicate their geometry. This segmented characteristic has also been considered in static and dynamic modeling. RCSA model has been used for combining the measured dynamics of the tool holder/spindle and the analytically determined end mill modes. Both static and dynamic predictions are demonstrated to be extremely accurate for variety of cases. The approach presented here is very useful for implementation in a virtual machining system where the form errors and stability limits for a milling application can be determined automatically.

References

[1] Y. Altintas, Manufacturing Automation, Cambridge University Press, 2000.
[2] E. Budak, Y. Altintas, Identification of peripheral milling conditions for improved dimensional accuracy, International Journal of Machine Tools and Manufacture 34 (7) (1994) 907–918.
[3] F. Koenigsberger, J. Tlusty, Machine tool structures, Stability against Chatter, vol. I, Pergamon Press, 1967.
[4] S. Smith, J. Tlusty, An overview of modeling and simulation of the milling process, Transactions of the ASME Journal of Engineering for Industry 113 (1991) 169–175.
[5] F. Koenigsberger, A.J.P. Sabberwal, An investigation into the cutting force pulsations during milling operations, International Journal of Machine Tool Design and Research 1 (1961) 15–33.

[6] W.A. Kline, R.E. DeVor, I.A. Shareef, The prediction of surface accuracy in end milling, Transactions of the ASME Journal of Engineering for Industry 104 (1982) 272–278.
[7] E. Budak, Y. Altintas, Modeling and avoidance of static deformations in peripheral milling of plates, International Journal of Machine Tools and Manufacture 34 (3) (1995) 459–476.
[8] Y. Altintas, S. Engin, Generalized modeling of mechanics and dynamics of milling cutters, Annals of the CIRP 50 (2001) 25–30.
[9] Y. Altintas, E. Budak, Analytical prediction of stability lobes in milling, Annals of the CIRP 44 (1995) 357–362.
[10] E.J.A. Armarego, R.C. Whitfield, Computer based modeling of popular machining operations for force and power predictions, Annals of the CIRP 34 (1985) 65–69.
[11] S.A. Tobias, Machine Tool Vibration, Blackie and Sons Ltd, 1965.
[12] J. Tlusty, F. Ismail, Basic nonlinearity in machining chatter, Annals of the CIRP 30 (1981) 21–25.
[13] I. Minis, T. Yanushevsky, R. Tembo, R. Hocken, Analysis of linear and nonlinear chatter in milling, Annals of the CIRP 39 (1990) 459–462.
[14] E. Budak, Y. Altintas, Analytical prediction of chatter stability in milling-part I: general formulation; part II: application to common milling systems, Transactions of the ASME, Journal of Dynamic Systems, Measurement, and Control 120 (1998) 22–36.
[15] M.A. Davies, J.R. Pratt, B. Dutterer, T.J. Burns, Stability prediction for low immersion milling, Transactions of the ASME Journal of Manufacturing Science and Engineering 124 (2002) 217–225.
[16] T. Insperger, B.P. Mann, G. Stepan, P.V. Bayly, Stability of up-milling and down-milling, part 1: alternative analytical methods, International Journal of Machine Tools and Manufacture 43 (2003) 25–34.
[17] Y. Altintas, A. Spence, End milling force algorithms for CAD systems, Annals of the CIRP 40 (1991) 31–34.
[18] Z. Yazar, K.F. Koch, T. Merrick, T. Altan, Feed rate optimization based on cutting force calculations in 3-axis milling of dies and molds with sculptured surfaces, International Journal of Machine Tools and Manufacture 34 (3) (1994) 365–377.
[19] M. Weck, Y. Altintas, C. Beer, CAD assisted chatter free NC tool path generation in milling, International Journal of Machine Tools and Manufacture 34 (1994) 879–891.
[20] E. Budak, Y. Altintas, E.J.A. Armarego, Prediction of milling force coefficients from orthogonal cutting data, Transactions of the ASME Journal of Manufacturing Science and Engineering 118 (1996) 216–224.
[21] L. Kops, D. Vo, Determination of the equivalent diameter of an end mill based on Its compliance, Annals of the CIRP 39 (1990) 93–96.
[22] T.L. Schmitz, Predicting high speed machining dynamics by substructure analysis, Annals of the CIRP 49 (2000) 303–308.
[23] T.L. Schmitz, M.A. Davies, M.D. Kennedy, Tool point frequency response prediction for high speed machining by RCSA, Transactions of the ASME Journal of Manufacturing Science and Engineering 123 (2001) 700–7007.
[24] F. Beer, E. Johnston, Mechanics of Materials, McGraw-Hill, UK, 1992.
[25] J.A. Nemes, S. Asamoah-Attiah, E. Budak, Cutting load capacity of end mills with complex geometry, Annals of the CIRP 50 (1) (2001) 65–68.
[26] E. Kivanc, E. Budak, Development of analytical end mill deflection and dynamic models, Proceedings of ASME IMECE Conference, IMECE 2003-42301, Washington, DC, USA, November, 2003.
[27] B. Jorgensen, Y. Shin, Dynamics of spindle-bearing systems at high speeds including cutting load effects, Transactions of the ASME Journal of Manufacturing Science and Engineering 120 (2) (1998) 387–394.
[28] T. Schmitz, Burns, Receptance coupling for high speed machining dynamics prediction, Proceedings of the 2003 International Modal Analysis Conference (IMAC-XXI), Kissimmee, FL, 2003.
[29] MathWorks, Mathlab 6.5.0 Relase 13: High Performance Numeric Computation and Visualization Software, Naatick, MA, 2002.